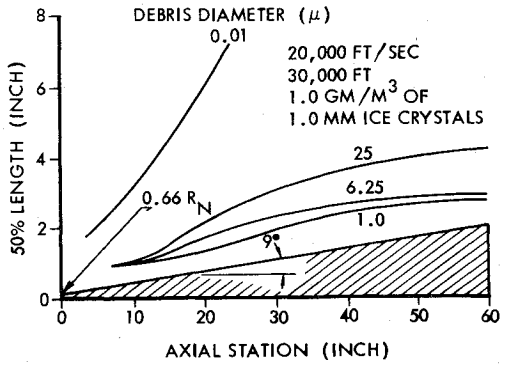

Fig. 4 50% length distributions.

$$V_{x\,rel} = V_I \cos\theta_p - V_d \cos\theta_b \tag{9}$$

$$V_{y\,rel} = V_I \sin\theta_p - V_d \sin\theta_b \tag{10}$$

Neglecting particle cross-section area change and the probability of colliding with more than one bubble from any single segment, the average mass of a particle impacting the *kth* segment is

$$m_{plk} = m_{pok} - \sum_{j=1}^{k} (1 - P(0)_{jk})\,\Delta m_{pjk} \tag{11}$$

Results

A typical re-entry vehicle and particle environment were analyzed. Debris fragment diameters from 0.01 to 25 μ and cloud densities from 0.1 to 1.0 gm/m^3 were studied. Figures 2 and 3 show the probability of a particle encountering debris fragments from any upstream segment (e.g., unity minus the probability shown is the probability that a particle would encounter no debris fragments).

The results of the particle mass loss calculations for the previous cases indicate that debris shielding at any point on the body is dominated by debris generated immediately upstream from that point. To provide a more convenient parameter for studying the upstream extent of the region providing significant shielding of a point, the "50% length" is defined as the upstream extent of the segment that produces 50% of the debris shielding of that point. Figure 4 shows the variation in 50% length along a re-entry vehicle for debris fragments sizes from 0.01 to 25 microns. Since heatshields are reinforced typically with filaments that are on the order of 10 μ in diameter, it would be expected that a large fraction of the debris would be in that size class. Since Fig. 4 shows that for fragments larger than 1.0 μ the 50% length never exceeds 4 in., it appears that debris shielding is dominated by slow-moving debris fragments. This is analogous to the stagnation region debris shielding and implies that stagnation point shielding correlations might be applicable to heatshields also.

The previous analysis was repeated assuming that the debris fragments from each upstream body segment were distributed uniformly in the debris layer rather than being confined to discrete bubbles. Interestingly, the 50% length predictions vary little from those shown above.

References

[1] Reinecke, W.G., "Debris Shielding During High-Speed Erosion," *AIAA Journal*, Vol. 12, Nov. 1974, pp. 1592-1594.

[2] Smith, D.H., "A Computer Analysis of Shock Layer/Particle Interactions," PDA Rept. TB 4001-00-01, 15 April 1974, Prototype Development Associates, Inc., Santa Ana, Calif.

Viscous Flow Around Close-Fitting Spherical Pistons in Right Circular Cylinders

G. David Huffman*
Indianapolis Center for Advanced Research and Indiana-Purdue University at Indianapolis, Ind.

Introduction

HYDRAULIC actuators, pumps and motors, and hydrostatic transmissions which are utilized in both air and ground transportation systems can be reduced in cost by using a small-clearance spherically ground piston within a right circular cylinder. The use of this concept eliminates the need for a wrist-pin and intricate sealing mechanisms resulting in decreased costs. To obtain maximum efficiency from these units, it will be necessary to provide a piston-cylinder clearance which will limit the leakage losses past the piston due to the pressure differential without incurring excessive torque loss from viscous shear forces and mechanical friction. The purpose of this Note is to both predict and measure the leakage flow and frictional characteristics of spherical pistons in close fitting cylinders as a function of imposed pressure difference, piston velocity, clearance, eccentricity, and fluid viscosity.

Experimental Apparatus

The experimental program was carried out in two phases. The first phase consisted of determining the flow past a close fitting spherical piston in a cylinder subjected to an imposed pressure difference. This experiment is similar to Poiseuille[1] flow in that both the piston and cylinder were fixed and a pressure differential applied. The objective of the second experiment was to determine the viscous shear and mechanical frictional forces encountered when the close-fitting spherical piston moves at high speeds within the cylinder. This phase is analogous to Couette[1] flow wherein the piston is moved at constant velocity and no external pressure differential is imposed.

In an actual application both of the previous processes occur simultaneously. The two conditions are dealt with separately in the experimental program in order to simplify the apparatus. The two effects are combined theoretically using a mathematical model developed in this Note.

A test apparatus was fabricated to measure oil leakage past the piston as shown in Fig. 1. Test cylinders and test pistons of different diameters were manufactured to cover the clearance range of interest. The cylinder nominal diameter was 2.00 in (5.08 cm) with clearance values, i.e., $\Delta r / r_i$, of 0.85×10^{-4}, 1.40×10^{-4}, 1.85×10^{-4}, 2.40×10^{-4}, and 3.40×10^{-4}, where r_i is the cylinder inner radius and Δr is the piston-cylinder clearance.

The spherical piston was installed on a tie-rod in the test fixture to permit adjustment of the piston within the cylinder. A pump in conjunction with an accumulator was used to supply hydraulic fluid to the test apparatus. The hydraulic fluid was filtered prior to entering the test apparatus to prevent foreign material from being trapped in the piston-cylinder annulus

Received February 21, 1975; revision received July 29, 1975. The author would like to acknowledge the assistance of B. L. McKamey and W. A. Bennett of the Research Dept., Detroit Diesel Allison Div., General Motors Corp., in carrying out the experimental investigations.

Index categories: Viscous Nonboundary-Layer Flows; Aircraft Subsystem Design.

*Center Fellow and Professor of Applied Mathematics. Associate Fellow AIAA.

and effectively reducing the clearance. A water-cooled heat exchanger was installed in the pump bypass to maintain a constant fluid temperature. Leakage and/or through flow rates were determined by measuring the volume of hydraulic fluid or oil discharged in a timed interval.

The Couette flow experiments were carried out in a second test apparatus. This assembly is shown in Fig. 2 and again utilizes a spherical piston and right circular cylinder. The piston was attached to a cross-head rod and was given a reciprocating motion. The crank and rod assembly were driven by an electric motor. The piston maximum velocity was adjusted from approximately 4-11 fps (1.2-3.4 m/sec). Note that the piston-cylinder is not pressurized and thus no pressure gradient is imposed.

The cylinder nominal diameter was again 2.00 in. (5.08 cm) with 3 cylinders fabricated to provide clearance values of 1.2×10^{-4}, 2.1×10^{-4}, and 3.4×10^{-4}. The cylinder was supported by a strain gage arm through one pivot point; consequently, the cylinder was free to align itself concentric with the piston and parallel to the piston travel. The force measurements were obtained via the strain gage assembly of Fig. 2.

Experimental Investigations

The experimental investigations were carried out sequentially in the facilities shown in Figs. 1 and 2. The Poiseuille measurements were conducted first using the piston-cylinder combinations as previously described. Prior to installation in the test apparatus, the diameter and surface finish of both the pistons and cylinders were measured. These elements were then installed in the fixture and the leakage rate was measured for each piston-cylinder combination with the piston centered in the cylinder, i.e., $e=0$, and with the piston moved fully to one side or contacting the cylinder, i.e., $e=\Delta r_0$ where e denotes the eccentricity, and Δr_0 the minimum clearance.

A range of Reynolds numbers was generated by utilizing a series of fluids having varying viscosities. The fluid viscosities were all experimentally determined and varied from 0.652×10^{-2} to 3.531×10^{-2} lb_m/ft-sec (0.097-0.525 gm/cm-sec).

The Couette flow experiments were carried out in a similar manner with piston-cylinder diameters again measured prior to installation in the test apparatus. Since the piston-cylinder assembly was self-aligning in this case, only eccentricity values of zero were evaluated. Drag coefficients were computed from the measured strain.

Theoretical Investigation

To minimize the data required, maximize the range of validity of the resulting model and combine the measured leakage flow and friction values for Poiseuille and Couette flow, a theoretical study was undertaken to parallel the experimental investigations. Analyses of sphere-in-cylinder systems have been carried out by many different investigators. In particular, Floberg[2] and Happel and Brenner[3,4] considered the flow around spheres contained in cylinders. The models of these references are not directly applicable to the problem at hand and thus a quasi-integral solution was developed.

An exact analysis of the sphere-cylinder flowfield would include all three of the equations of motion, the continuity equation, and the energy equation. The solution of this system of equations would be extremely difficult if not impossible to obtain. As a result of these difficulties, the equations were simplified using an order-of-magnitude analysis. This yielded

$$0=-\partial p/\partial x+(1/r)(\partial/\partial r)[\mu r(\partial u_x/\partial)] \quad (1)$$

$$0=-\partial p/\partial r=-\partial p/\partial\theta \quad (2)$$

$$0=(1/r)(\partial r u_r/\partial r)+(\partial u_x/\partial x) \quad (3)$$

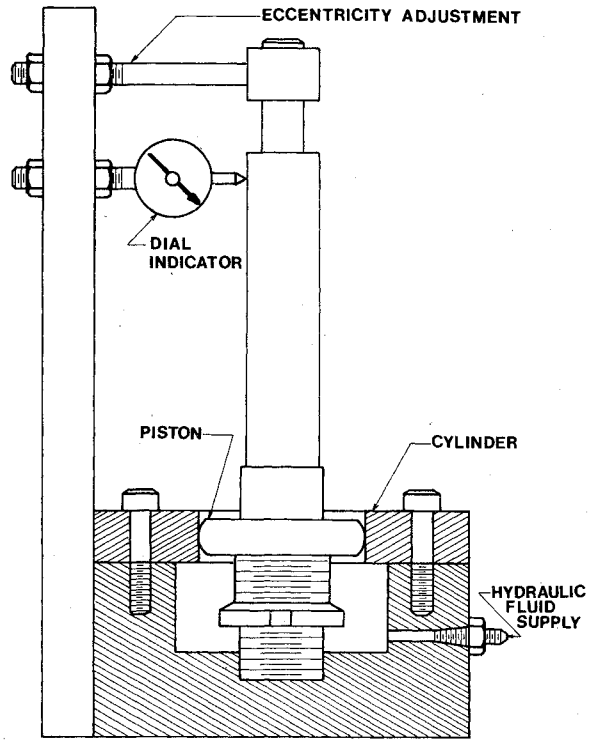

Fig. 1 Schematic diagram of the test apparatus for measuring the leakage flow past a spherical piston.

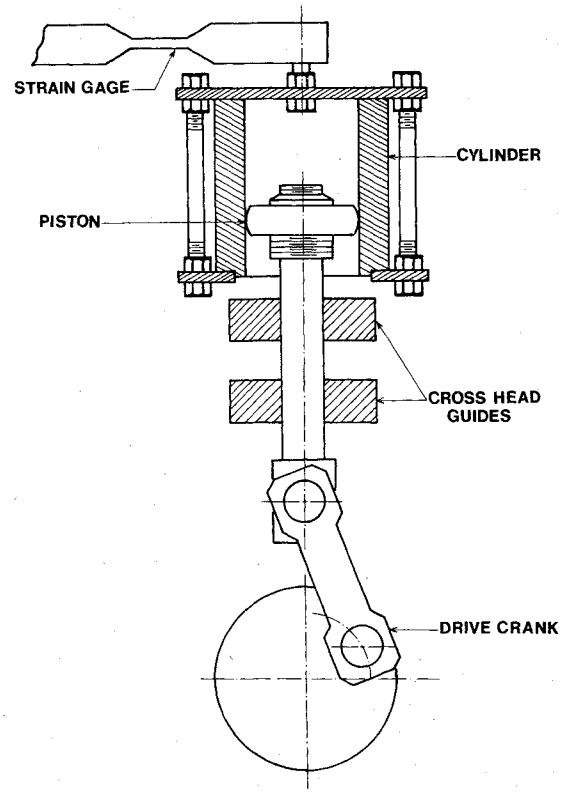

Fig. 2 Schematic diagram of the test apparatus for measuring the sphere-piston friction.

$$t=t_c \quad (4)$$

where u_x and u_r denote the axial and radial velocity components, p the static pressure, t the static temperature, μ the absolute viscosity, and x,r,θ the cylindrical coordinates. Equation (2) implies that the static pressure varies only in the

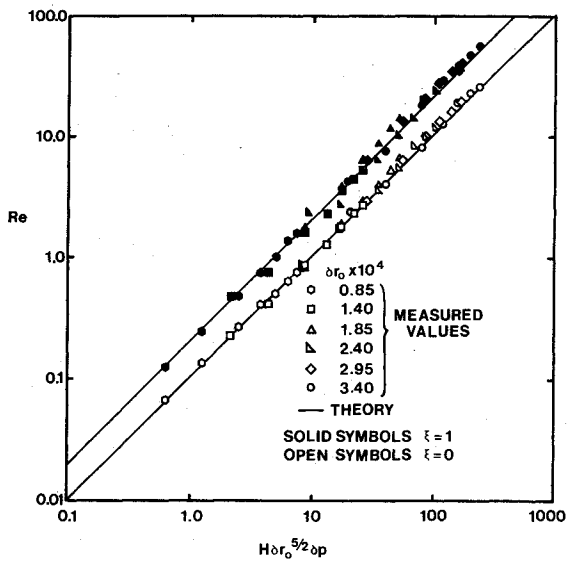

Fig. 3 Reynolds number vs $H\delta r_0^{5/2}\delta p$ for varying values of δp, δr_0, ξ, and H.

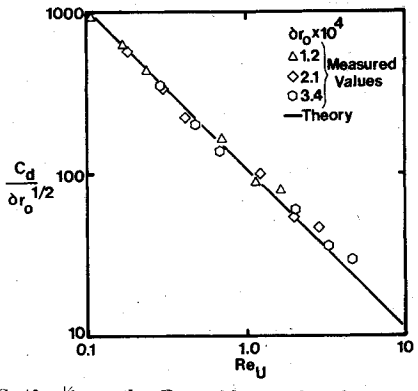

Fig. 4 $C_d/\delta r_0^{1/2}$ vs the Reynolds number for a centered piston-sphere configuration.

axial direction. This fact combined with an integral continuity condition

$$\int_0^{2\pi}\int_{r_i-\Delta r}^{r_i} u_x r dr d\theta = q \tag{5}$$

yields a system of differential equations describing the flowfield. Equations (1) and (5) are solved for the volumetric flow rate q with an imposed pressure differential Δp and/or piston motion U. The viscous drag can then be derived and is

$$F_x = -\int_{-\infty}^{\infty}\int_0^{2\pi} \mu(\partial u_x/\partial r)_{r_i-\Delta r}(r_i-\Delta r)\,d\theta dx \tag{6}$$

where F_x denotes the axial viscous force.

Equations (1), (5) and (6) can be integrated provided Δr and the appropriate boundary conditions, i.e., $r=r_i$, $u_x=0$, $r=r_i-\Delta r$, $u_x=U$ are specified. The pressure gradient term can be linked to the volumetric flow rate via the integral continuity condition and

$$\frac{H\delta p \delta r_0^{5/2}}{\pi} = \frac{8Re}{\sqrt{2}\xi^2}\left[1-\frac{(1+[1+3/2\xi^2]^{1/2})^{1/2}}{(2+3\xi^2)^{1/2}}\right] - \frac{3Re_U}{(1+3/2\xi^2)^{1/2}[1+(1+3/2\xi^2)^{1/2}]^{1/2}} \tag{7}$$

A similar relationship can be obtained for viscous and/or frictional force and

$$\frac{Re_U^2 C_d}{\pi\delta r_0^{1/2}} = \frac{12Re_U[1+(1+3/2\xi^2)^{1/2}]^{1/2}}{(1+3/2\xi^2)^{1/2}} - \frac{24Re}{(1+3/2\xi^2)^{1/2}[1+(1+3/2\xi^2)^{1/2}]^{1/2}} \tag{8}$$

Note that $Re=q\rho/\pi r_i\mu$, $Re_U=2r_i\delta r_0\rho U/\mu$, $\delta r_0=\Delta r_0/r_i$, $\xi=e/\Delta r_0$, $\delta p=\Delta p/p_r$, $C_d=F_x/\pi r_i^2\rho U^2$, $H=r_i^2\rho p_r/\mu^2$, where ρ denotes the fluid density, and p_r a reference pressure.

Comparison of Theoretical and Experimental Results

The results of the Poiseuille flow experiments are shown in Fig. 3. The theoretical relationship is also shown indicating that Eq. (7) is sufficient to correlate the data over a wide range of operating conditions. The deviation between predicted and measured results is greater with increased Reynolds number. This deviation is generally attributed to inertia effects[1,5] and/or variation in fluid properties.

The Couette flow experimental apparatus, Fig. 2, was used to determine drag coefficient values. These data are plotted in Fig. 4 and are compared to the theoretical values of Eq. (8). This relationship was maintained throughout the range of test conditions implying the existence of a lubricating film between the piston and cylinder for all configurations. Again the theoretical and experimental results tend to diverge at larger Re_U values which is probably due to inertia effects.

Summary

Experimental investigations were carried out demonstrating the feasibility of using spherical pistons in right circular cylinders having very small clearances. A lubricating film was maintained in the most severe cases with piston-cylinder friction at acceptable levels. An analytic model was derived for this flow case using the assumptions of low Reynolds number and very small clearances. The experimental and theoretical results were in general agreement through the range of values appropriate for practical applications of the device.

References

[1]Schlichting, H., *Boundary Layer Theory*, McGraw-Hill, New York, 1960, pp. 66-74.

[2]Floberg, L., "On the Ball Flowmeter and the Ball Viscosimeter," *Acta Polytechnica Scandinavica*, Mechanical Engineering Series No. 36, 1968.

[3]Happel, J. and Brenner, H., *Low Reynolds Number Hydrodynamics with Special Applications to Particulate Media*, Prentice-Hall, New York, 1965, pp. 298-328.

[4]Brenner, H. and Happel, J., "Slow Viscous Flow Past a Sphere in a Cylindrical Tube," *Journal of Fluid Mechanics*, Vol. 4, 1958, pp. 195-213.

[5]McNown, J. S., Lee, H. M., McPherson, M. B., and Engez, S. M., "Influence of Boundary Proximity on the Drag of Spheres," *Proceedings of the Seventh International Congress of Applied Mechanics*, Vol. II, Pt. 1, London, 1948, pp. 17-29.

Preston Tube Calibration Accuracy

Arild Bertelrud*

FFA, The Aeronautical Research Institute of Sweden, Bromma, Sweden

Introduction

A large number of methods exists for measuring local skin friction, direct ones using a skin friction bal-

Received May 5, 1975; revision received August 28, 1975. This investigation was sponsored by the Swedish Material Administration of the Armed Forces, Air Material Department.

Index category: Boundary Layers and Convective Heat Transfer-Turbulent.

*Research Engineer. Member AIAA.